PAPER • OPEN ACCESS

The effect of neon seeding on plasma edge transport in EAST

To cite this article: Dieter Boeyaert *et al* 2025 *Nucl. Fusion* **65** 106029

OPEN ACCESS
IOP Publishing | International Atomic Energy Agency
Nuclear Fusion
Nucl. Fusion **65** (2025) 106029 (20pp)
https://doi.org/10.1088/1741-4326/ae05b0

The effect of neon seeding on plasma edge transport in EAST

Dieter Boeyaert[1,2,3,*], Stefano Carli[2], Wouter Dekeyser[2], Sven Wiesen[3,4], Liang Wang[5], Fang Ding[5], Kedong Li[5], Yunfeng Liang[3,5], Martine Baelmans[2] and the EAST Team[a]

[1] Department of Nuclear Engineering and Engineering Physics, University of Wisconsin-Madison, 1500 Engineering Drive, Madison, WI 53706, United States of America
[2] Department of Mechanical Engineering, KU Leuven, Celestijnenlaan 300, 3001 Leuven, Belgium
[3] Forschungszentrum Jülich GmbH, Institut für Energie- und Klimaforschung—Plasmaphysik, 52425 Jülich, Germany
[4] DIFFER—Dutch Institute for Fundamental Energy Research, De Zaale 20, 5612 AJ Eindhoven, Netherlands
[5] Chinese Academy of Sciences, Institute of Plasma Physics, Hefei 230031, China

E-mail: boeyaert@wisc.edu

Received 4 May 2025, revised 21 August 2025
Accepted for publication 10 September 2025
Published 23 September 2025

Abstract

Impurity seeding is crucial for power exhaust in future power plants. In the presented analysis, neon seeding for the Experimental Advanced Superconducting Tokamak (EAST) tokamak is studied. Experiments from the 2019 campaign are taken as a starting point for SOLPS-ITER simulations. In a next step, these simulations are used to study the effect of neon seeding in EAST. It is shown that drift flows are crucial to predict correctly where the ionization sources are located and determines the stagnation point, both for the main ion species (deuterium) as for the neon impurities. Line radiation of neon is only a major contribution to the radiated power fraction when detachment is achieved. In the other cases neutral radiation, and radiation due to background impurities (in the simulations assumed as a carbon–oxygen mixture) is dominating the radiation. This large neutral radiation indicates the importance of neutral transport. In the simulations elastic collisions, ionizing dissociation and charge exchange are considered. Volumetric recombination does not play an important role, even not in the detached simulation. Comparison with findings on other devices shows that the observed patterns are similar. The transport analysis shows that Ne^{+} leaks towards the core explaining why it is difficult to perform experiments with only neon as a radiative species for EAST-size devices.

Keywords: EAST, SOLPS-ITER, neon, detachment, drifts, radiation, neutral transport

(Some figures may appear in colour only in the online journal)

[a] See Gong *et al* 2024 (https://doi.org/10.1088/1741-4326/ad4270) for the EAST Team.
[*] Author to whom any correspondence should be addressed.

1. Introduction

For future fusion devices, it is a challenge to control the heat and particle exhaust [1]. In order to keep the heat loads limited, a detached plasma state is required [2]. Plasma is detached by modifying edge transport as such that the plasma particles lose a large part of the energy and momentum they are carrying before interacting with the divertor targets. The reduced temperature of the plasma makes that the plasma facing components are shielded (detached) from the hot plasma by a small neutral layer [3–5].

To avoid dilution of the plasma due to sputtered impurities, it is desirable to detach the plasma from the wall. This is called a detached plasma state and is determined by the physics the plasma particles experience traveling from the upstream location at the outer midplane (OMP) – where most plasma particles escape from the core—to the downstream location at the divertor targets. An overview of these processes is given in figure 1.

At low densities, heat transport is dominated by the convection through the sheath at the divertor targets [6]. In this regime the plasma quantities stay constant in the bulk plasma edge and only large gradients in temperature and density are happening in the sheath itself. This is called the low recycling or sheath-limited plasma regime. When the density is increased, the conduction zone indicated in figure 1 will start creating larger gradients in the temperature and density between up- and downstream bringing the plasma in the high recycling or conduction limited regime [7]. If the density keeps increasing, there comes a point where the downstream temperature drops sufficient to make that radiation from (light) impurities contributes to the energy loss and in that way to the temperature drop between up- and downstream. Figure 1 shows that a radiation zone appears when the plasma temperatures drop down to around $\sim$10 eV around the X-point. The strength of the radiation and the exact temperatures at which it takes place depend on the specific impurity [8]. If this impurity radiation cools down the plasma sufficiently to temperatures of $\sim$5 eV, the main ion (hydrogen or deuterium) ionization zone is formed further downstream and cools down further the plasma as indicated in figure 1. This results in a poloidal plasma flow towards the targets. As the neutral density keeps increasing when coming closer to the divertor target, neutral friction becomes important. The key processes behind this neutral friction are elastic collisions and charge exchange between the hydrogen or deuterium neutrals and the plasma particles. This causes that the plasma particles lose parallel momentum and in that way that the flow velocity towards the targets is reduced. Close to the divertor target, where the low flow velocity causes that the transit time is similar to the recombination time, volumetric recombination takes place. As indicated in figure 1 the plasma temperatures should be low before volumetric recombination takes place, around $\sim$1 eV. Depending on the plasma temperatures and densities along this path, all these transport mechanisms happen, or only some of them play a role.

For the onset of detachment, impurity radiation, ionization, neutral friction and recombination play a crucial role. It is possible to study the degree of detachment based on the observed phenomena [4]: when a reduction in heat flux on the targets is observed, energy detachment takes place, when the rollover in ion flux toward the target—a change from increasing to decreasing ion flux when the upstream density goes up—takes place, momentum detachment is happening, and when volumetric recombination shields the plasma from the target, also particle detachment is taking place leading to a further reduction in ion flux towards the targets. Where impurity radiation is the driver for energy detachment, the required loss in parallel momentum for momentum detachment is mainly caused by neutral friction, where volumetric recombination is the key mechanisms for particle detachment.

Extrinsic impurity seeding is often used to induce detachment as it helps to increase the radiation losses [9]. Impurities with a lack of surface chemistry like noble gases or low-Z elements are key candidates as they radiate at temperatures which are achieved in the scrape-off layer (SOL) and pedestal of the plasma.

An interesting low-Z element, is neon (Ne). Recently, large tokamaks like JET have shown to handle Ne seeding in H-mode in a metallic environment [10] and Ne is considered for ITER and DEMO [9]. Apart from JET, EAST (Experimental Advanced Superconducting Tokamak) is the only tokamak with a tungsten divertor in which Ne-seeding detachment experiments have been performed successfully without adding other radiators. EAST is a superconducting tokamak located at ASIPP in Hefei, China [11]. It has a major radius of 1.7 m and a minor radius of 0.4 m. During the experimental campaign of 2019, EAST was equipped with a tungsten upper divertor and a carbon lower divertor.

The current paper analyzes more in detail the effect of Ne seeding on the different plasma edge transport mechanisms of figure 1. As experimental data are limited, especially to investigate the influence of neon on the different processes, the focus is rather on SOLPS-ITER simulations. SOLPS-ITER is a 2D plasma edge code coupling the B2.5 code solving the Braginskii equations for the ions and electrons, to the EIRENE code solving the Boltzmann equations for the neutrals [12, 13]. Two discharges, a reference discharge in H-mode (shot number 87626) and a similar discharge with the maximum added amount of Ne to keep the discharge in H-mode (shot number 87628), are taken as a starting point. The experimental data are used to constrain the simulation setup, where the remaining analysis is mainly based on the simulations themselves.

Section 2 describes the investigated experiments and the setup for the SOLPS-ITER modeling. The up- and downstream profiles are discussed in section 3. A description of the effect of drifts on the plasma quantities in section 4 is followed by a study of the effect of neon on the radiated power fraction in section 5. Section 6 discusses the impact of neutrals on the plasma transport. The final section discusses the overall effects of neon seeding on the plasma before coming to the summary and conclusion.

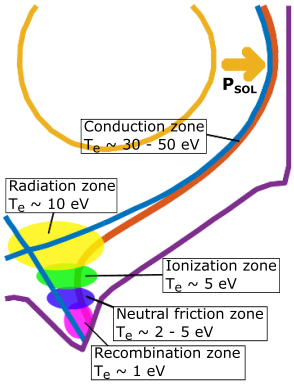

Figure 1. The path that the plasma particles and power follow while traveling from the core towards the divertor targets. The physical processes which take place on its way determine the plasma state.

2. Case description

The performed analysis is based on two EAST discharges in upper single null (USN) configuration, performed during the campaign of 2019, and described in [14]. The two investigated discharges (87626 without seeding and 87628 with Ne seeding) are H-mode experiments to which a total heating power of 2.25 MW was applied. The magnetic field was 2.5 T and the plasma current 400 kA. Deuterium was injected at the OMP using a feedback loop to keep the electron density at the separatrix constant ($n_{e,\mathrm{sep}} \sim 0.9 \cdot 10^{19}\mathrm{m}^{-3}$). Due to the used control system for the magnetic field, USN discharges in EAST are in fact disconnected double null (DDN) discharges with a large separation $\mathrm{dr}_{\mathrm{sep}}$. In the studied experiments $\mathrm{dr}_{\mathrm{sep}} \sim 2.5\,\mathrm{cm}$ as shown in figure 2(*b*). In shot 87628 Ne seeding was added in a 50% Ne, 50%D_2 mixture at the strike point in the upper outer target (UOT). Ten pulses of this Ne–D_2 mixture were added as shown in figure 2(*c*) and afterwards the plasma state (discharge 87628) is compared with the case in which no seeding was added (discharge 87626). The length of a Ne injection is in total 10 ms, from which 5 ms flattop. An overview of the main discharge parameters is given in figure 2. In figure 2(*a*) the input power for the experiment—a combination of LHW and ECRH heating—is shown, and in figure 2(*b*) the separation between the upper and lower separatrix is shown together with the H98 confinement plot for the studied discharges. Figure 2(*c*) shows the radiated power fraction for the studied discharges together with the Ne injection in shot 87628. Figure 2(*d*) shows the spectrometer data for different impurities in the performed experiments.

The setup for the SOLPS-ITER simulations is based on the one in [14–16]. As in these references, the 3.0.7 master version of the code is used. Although that the experiments are in fact carried out in a DDN configuration, the simulations use a USN setup and are limited to 2.5 cm outside the last closed flux surface. At the core boundary of the plasma grid, the density is imposed for the continuity equation of the deuterium ions: $n_i = 2.8 \cdot 10^{19}\ \mathrm{m}^{-3}$ based on the OMP profiles of the Thomson scattering (TS) system of EAST [17] discussed in section 3. The simulated Ne puff is located at the strikeline location at the UOT. Figure 2(*c*) indicates that 10 puffs of 10 ms each (5 ms flattop) with a puffed Ne fraction of 10^{20} particles s^{-1}. As this is a pulsed injection and as SOLPS-ITER is a steady-state code, these puffs are added to come to a total injection of $\sim 7.2\,10^{18}$ particles s^{-1}. This assumes that all Ne has an effect at the same time. As the Ne is injected in a Ne–D_2 mixture, a similar puff for D_2 is added to the Ne-seeded simulation. From the neon ions there is no exact measurement of each ion individually. As the TS profiles do not show a large increase in electron density at the core boundary of the grid, it is assumed that the lower charge states of neon are fully ionized and that their density is zero. For Ne^{5+}–Ne^{8+} small amounts in the range of $n_i = 5.0 \cdot 10^{14}\ \mathrm{m}^{-3}$ to $n_i = 2.0 \cdot 10^{17}\ \mathrm{m}^{-3}$ are imposed at the core boundary. Higher charge states are assumed not to be present. The deuterium level at the OMP is imposed through a feedback loop ($n_{e,\mathrm{sep}} = 0.9 \cdot 10^{19}\ \mathrm{m}^{-3}$) and kept similar for both simulations. Such a feedback loop makes the overall simulation and especially the inclusion of drifts more challenging from a numerical viewpoint [16]. The input power to the simulation is imposed as a boundary condition for the ion and electron energy equations. It is assumed that power is equally spread over ions and electrons. As boundary condition, the input power in the experiment, shown in figure 2(*a*) is decreased with the radiated power fraction given in figure 2(*c*). For the purely deuterium simulation, this results in an input power of 2.05 MW. As deuterium is radiating further downstream, no edge radiation within the viewing cords of the AXUV system are expected. Ne, on the other hand, will also radiate around the OMP. Therefore, not the full 0.6 MW of figure 2(*c*) is subtracted from the 2.25 MW input power, but only 0.45 MW is assumed to be core radiation resulting in an input power of 1.8 MW for the simulation. Figure 2(*d*) indicates that also other species are radiating. As the goal of the presented research is to investigate the effect of neon, these species are not included in the SOLPS-ITER simulations. At the targets, Bohm–Chodura conditions are applied and a recycling coefficient of one is imposed for all ions. More details about the used boundary conditions can be found in [15, 16]. Anomalous transport is imposed ad-hoc according to the profiles of figure 3. Similar anomalous transport is assumed for all species. Grid information can be found in [15, 16].

In SOLPS-ITER, the neutral kinetics are handled by the EIRENE code [18]. The included neutral reactions in the performed simulations are given in table 1. The reactions at the bottom of the table are only included in the neon simulations. It should be remarked that the included Ne ionization reaction is based on the coronal rate. As shown in [19] the use of collision-radiative rates instead of the coronal rates, will shorten the ionization length. This can influence the impurity leakage and should be considered while evaluating the simulation results.

All the presented simulations have fully activated $E \times B$ and diamagnetic drifts except when explicitly mentioned. This makes it the first time that EAST simulations with SOLPS-ITER and Ne seeding are studied with fully activated drifts. The direction of the different drift terms can be found in figure 4.

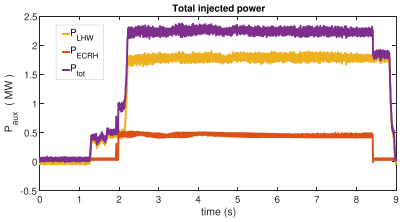

(a) The injected power during the discharges. A total power of $\sim 2.25\,\mathrm{MW}$ was injected existing of $\sim 1.80\,\mathrm{MW}$ LHW and $\sim 0.45\,\mathrm{MW}$ ECRH.

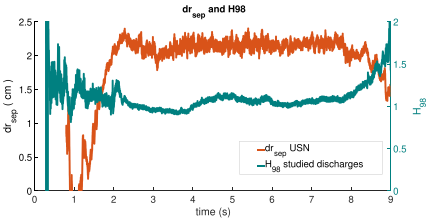

(b) $\mathrm{dr_{sep}}$ during the performed discharges (left axis) and the H98 profile which was similar for all discharges (right axis).

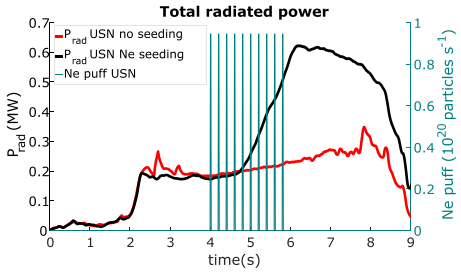

(c) The core radiated power fraction measured with the AXUV system for the reference discharge (no seeding) and during Ne seeding. On the right axis the injected amount of Ne is displayed.

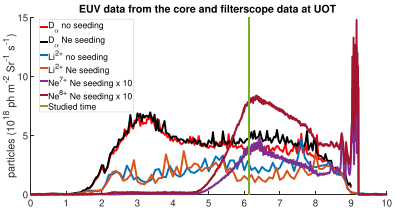

(d) The line emission at the UOT measured with the filterscope for D_α and Li^{2+} for the reference discharge (no seeding) and during Ne seeding. The line emission from the core measured with the EUV is shown for Ne^{7+} and Ne^{8+} during the neon seeded discharge. The investigated time slot in both experiments is indicated in green.

Figure 2. Overview of the main experimental parameters for the studied discharges in this paper.

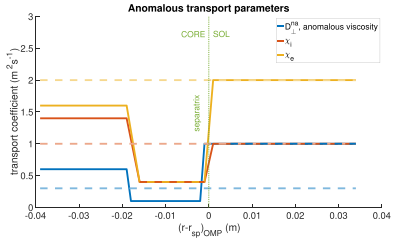

Figure 3. Overview of the transport coefficients used in the presented SOLPS-ITER simulations. The transport coefficients in the divertor and private flux regions are shown with dotted, more transparent curves.

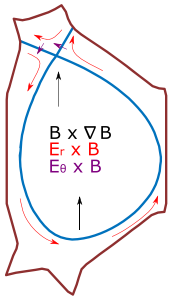

Figure 4. The direction of the $E \times B$ and diamagnetic drifts.

3. Upstream and downstream profiles

Key parameters to study plasma edge transport in both simulations and experiments are the upstream plasma conditions at the OMP, and the downstream ones at the inner and outer targets (UIT and UOT) [6, 7].

As mentioned in the previous section, the upstream data are measured with the TS system. For the downstream experimental data, the divertor Langmuir probes (DivLPs) from EAST are used [20].

As EAST is used for long pulse operations and due to the triple probe setup, it is difficult to have always correct measurements. In case there are indications that the probe tip area is damaged, or if one of the voltage signals does not react on changes in the plasma, the data are excluded. The most reliable measurements are the j_s profiles (only dependent on current measurement and probe tip area), and the T_e ones (only dependent on two voltage measurements).

As no ELM-filtering is available for the DivLP data, the median of five data points, 50 ms apart from each other around the studied time in the discharge is taken to avoid the influence of ELMs on the measured profiles. Error bars of 20% are assumed for all DivLP profiles [20]. They, however, do not count for problems with the voltage measurements or damaged probe tips. Similar ELM-filtering for the TS data is not possible as only few measurements per discharge are available.

In the performed analysis toroidal symmetry is assumed. Figure 5, however, shows that an asymmetry between measurements at different ports is present. As the presented work aims to investigate the effect of Ne seeding on the plasma transport, rather than having an exact comparison between experiments and simulations, simulations are only compared to the experimental target data at port D. Port D was chosen as the initial comparison with the simulations in [14] was performed for this port.

The upstream OMP n_e and T_e profiles are obtained from the TS system which is installed at port L of the EAST

Table 1. The included neutral reactions in the EIRENE mode for deuterium and neon.

Reaction	Reaction type	Reference
$D + D \rightarrow D_2^+ + e$	Elastic collision	AMMONX H.2 R-H-H
$D + D_2 \rightarrow D_3^+ + e$	Elastic collision	AMMONX H.2 R-H-H2
$D + e \rightarrow D^+ + 2e$	Ionization	AMJUEL H.4,10 2.1.5
$D + D^+ \rightarrow D^+ + D$	Charge exchange	HYDHEL H.1,3 3.1.8
$D_2 + D \rightarrow 3\,D$	Elastic collision	AMMONX H.2 R-H2-H
$D_2 + D_2 \rightarrow D_2 + D + D$	Elastic collision	AMMONX H.2 R-H2-H2
$e + D_2 \rightarrow 2e + D_2^+$	Ionization	AMJUEL H.4 2.2.9
$e + D_2 \rightarrow e + D + D$	Dissociation	AMJUEL H.4 2.2.5 g
$e + D_2 \rightarrow 2e + D + D^+$	Ionizing dissociation	AMJUEL H.4 2.2.10
$D_2 + D^+ \rightarrow D^+ + D_2$	Elastic collision	AMJUEL H.0,1,3 0.3 T
$D_2 + D^+ \rightarrow D_2^+ + D$	Charge exchange	AMJUEL H.2 3.2.3
$e + D_2^+ \rightarrow e + D + D^+$	Dissociation	AMJUEL H.4 2.2.12
$e + D_2^+ \rightarrow 2e + D^+ + D^+$	Ionizing dissociation	AMJUEL H.4 2.2.11
$e + D_2^+ \rightarrow D + D$	Recombining dissociation	AMJUEL H.4,8 2.2.14
$D^+ + 2e \rightarrow D + h\nu$	Recombination	AMJUEL H.4,10 2.1.8
$e + Ne^{(x-1)+} \rightarrow e + Ne^{x+} + e$	Ionization	AMJUEL H.2 2.10B0
$Ne^{x+} + e \rightarrow Ne^{(x-1)+}$	Recombination	ADAS H.4,10 acd96,prb96

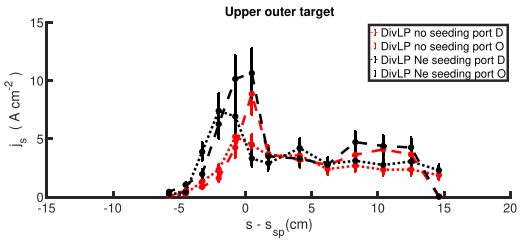

Figure 5. The DivLP data for the ion saturation current at the upper outer target. Data are taken at two toroidal locations (port D and port O).

device. Figure 6 shows a limited influence of the neon seeding on the experimental OMP profiles. Based on these experimental profiles, the experimental decay lengths for temperature and density are estimated to be: $\lambda_{T_e} \approx 4.5\,\text{mm}$ and $\lambda_{n_e} \approx 2.0\,\text{cm}$. As the SOLPS-ITER grid only extends slightly further into the SOL than λ_{n_e}, it has been verified in [16] that maximum $\sim$25% of the power is leaving the simulation domain through the grid boundary closest to the first wall. Initial simulations with a DDN setup were performed and showed similar trends to the ones with the USN setup, but it was not possible to get them fully converged. Therefore, they are not considered in the performed analysis.

Figure 6(*a*) shows that the slightly increased OMP density is captured by the SOLPS-ITER simulations (SOLPS D_2 1 and SOLPS Ne 1), but figure 6(*b*) illustrates that the effect of Ne seeding on the upstream temperature is overestimated in the SOLPS-ITER simulation.

The downstream simulation data (SOLPS D_2 1 and SOLPS Ne 1 in figures 8 and 9 indicate a limited influence of the neon on the simulation result: the overall profiles stay the same and only around the separatrix larger differences are observed. The experimental profiles, on the other hand, show a larger effect of neon. The maximum value for T_e at the UOT, for instance, only decreases with $\sim$8 eV in the simulation where the experiment indicates a decrease of more than 55 eV! Nevertheless, the observed trends in the experiment are similar to the simulated ones.

Therefore, the setup for the Ne-seeded simulation is changed to obtain the best possible agreement with the experiments (SOLPS Ne 2). For this later simulation, the transport profiles of figure 3 are replaced by the profiles in figure 7, the neon puff is increased with a factor 20, and also the upstream density is increased. It is unlikely that this level of Ne can be achieved in an H-mode experiment, but this made it possible to achieve better downstream agreement between simulations and experiments as shown in figures 8 and 9.

As mentioned before, figures 2(*c*) and (*d*) show that not only neon is a radiating impurity. As deuterium cannot radiate at the temperatures expected in the core, other radiators have to be present. Figure 2(*d*) indicates the presence of lithium in the vicinity of the UOT. In fact, several impurity species are expected in EAST plasmas [21]: the lower divertor, the shine-through area for the NBI, and the outboard guard limiters are from carbon, where the first wall is made from molybdenum. To reduce the impact of the carbon wall parts, but also to avoid hydrogen in a deuterium plasma and enable long pulse operation, lithium wall conditioning is used. The experimental data show, however, that this results in at least carbon, lithium and tungsten in the main plasma. As introducing these impurities as separate species in SOLPS-ITER will slow down the simulation, and as the focus of this work is on the effect of neon, the artificial radiation switch in SOLPS-ITER is used. In the 'SOLPS Ne 2' simulation, it is assumed that the concentration of this artificial radiator is 1% in the plasma. The effective radiation is then determined by: $P_{\text{rad,art.}} = 0.01 \cdot n_a n_e L(T_e)$ with n_a the deuterium density, n_e the electron density and L_{T_e}

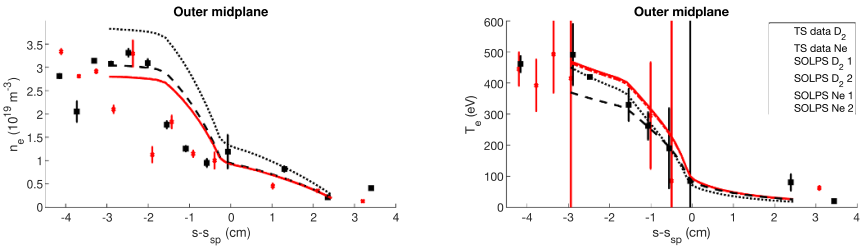

(a) The electron density profiles measured with the TS system and from the SOLPS-ITER simulations at the OMP.

(b) The electron temperature profiles measured with the TS system and from the SOLPS-ITER simulations at the OMP.

Figure 6. The upstream profiles at the OMP for electron density and temperature during the purely deuterium and neon seeded discharges and simulations.

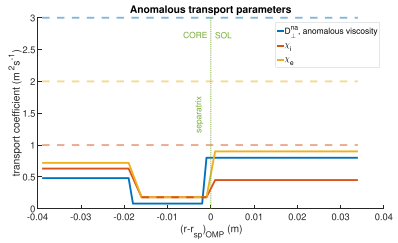

Figure 7. Overview of the transport coefficients used in the additional SOLPS-ITER simulation with neon impurities (SOLPS Ne 2). The transport coefficients in the divertor and private flux regions are shown with dotted, more transparent curves.

Table 2. Overview of the used simulations in this work and the changes to them in comparison with the initial deuterium simulation.

	D_2	Ne
SOLPS 1	Initial	Ne–D_2 injection
SOLPS 2	1% artificial radiation	·1% artificial radiation · Changed anomalous transport · Increased Ne–D_2 injection · Increased upstream density

the radiative loss function which is built-in in SOLPS-ITER and based on a mixture of carbon–oxygen. To also account for this additional radiation in the purely deuterium simulations, an additional deuterium simulation with 1% of this artificial radiator is performed (SOLPS D_2 2).

This brings the total number of examined simulations to four: two with deuterium ('SOLPS D_2 1' and 'SOLPS D_2 2') which are using the same simulation setup apart from the artificial radiation, one Ne simulation which has a similar SOLPS-ITER setup as the deuterium ones apart from the Ne–D_2 injection (SOLPS Ne 1), and a further elaborated Ne simulation with artificial radiation, and several changes to the simulation setup to match the downstream profiles at the UOT (SOLPS Ne 2). An overview of these simulations is given in table 2.

The included artificial radiation in simulation 'SOLPS D_2 2' lowers slightly the temperature at the UOT, but the spike in the j_s, n_e and as a result also in the q_t profiles right outside the separatrix, is largely increased.

Comparison of simulations 'SOLPS D_2 2' and 'SOLPS Ne 1', shows that the effect of adding the injected Ne–D_2 mixture to the simulation on the target profiles is similar (but not the same) as adding artificial radiation. This indicates that in both simulations the changes are determined by an additional radiated power fraction (see section 5) and the increased peak in the j_s profile of simulation 'SOLPS Ne 1' is not determined by the additional Ne–D_2 injection.

Simulation 'SOLPS Ne 2' manages to match better the experimental data at the UOT. This suggests that the amount of Ne in the device is larger than the injected amount (which is possible as other Ne experiments took place before discharge 87628, but it is unlikely there was 20 times as much Ne present), or that the anomalous transport profiles have changed. Therefore, also the transport physics of simulation 'SOLPS Ne 2' is analyzed in the next sections.

In SOLPS-ITER simulations of other devices, it was always possible to match the simulations with experiments by using the same anomalous transport coefficients for all species [22, 23]. This suggests that the observed experimental profiles in the case of neon seeding are influenced by more than only the injected neon. Possible causes are the presence of additional radiative species shown in figure 2(*d*), or the toroidal asymmetries causing locally larger or smaller effects due to neon.

In the remaining of this paper, the 'SOLPS Ne 1' simulation is used to study the effect of neon on its own and compare the findings for EAST with studies on other devices, where the 'SOLPS Ne 2' simulation is used to search an explanation of what is the largest effect which has experimentally been observed on EAST.

Based on the experimental profiles of figures 6 and 8, the one dimensional particle balance ($2n_tT_t = f_{\mathrm{mom}}n_uT_u$) with f_{mom} the momentum loss factor in the flux tube, is $f_{\mathrm{mom}} \approx 0.88$ and $f_{\mathrm{mom}} \approx 0.65$ in the neon seeded experiment. This indicates a larger momentum loss because of the neon seeding which is expected due to the decreased temperatures at the target. In fact, the decrease in maximum T_e at the UOT means that conduction becomes more important in comparison with the purely deuterium experiment as can be concluded from the temperature-dependent edge physical processes of figure 1.

The data at the UIT of figure 9 disagree for all cases between simulations and experiments. Especially the temperature at the inner target is extremely low in the simulations.

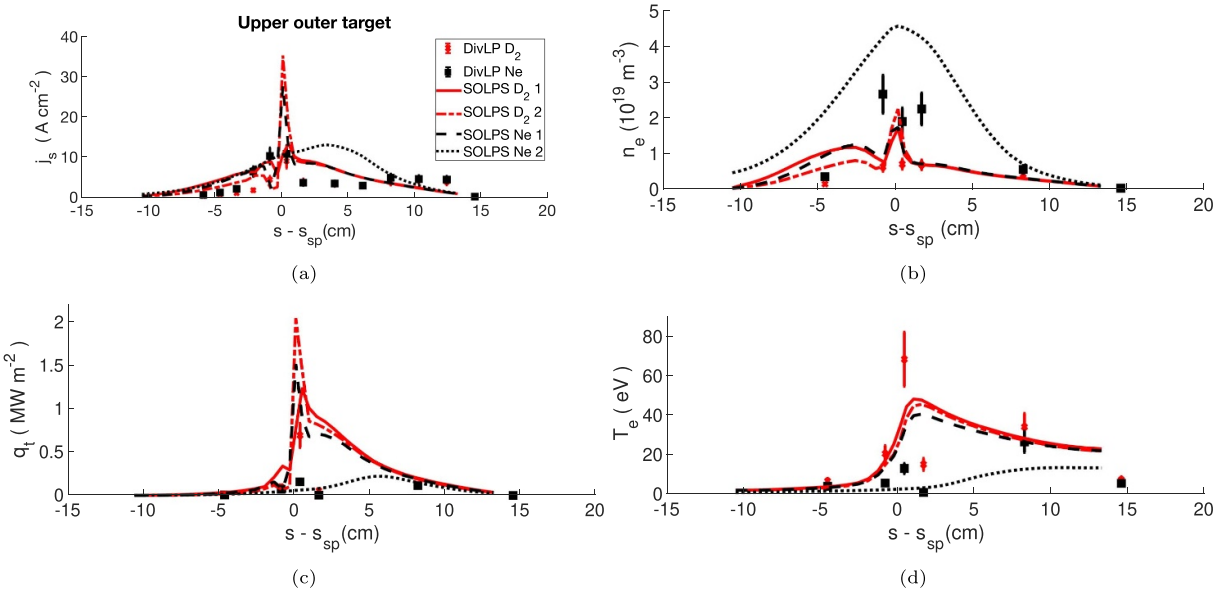

Figure 8. The profiles of the ion saturation current (*a*), density (*b*), heat flux (*c*) and temperature (*d*) at the UOT during the purely deuterium and the neon seeded discharge.

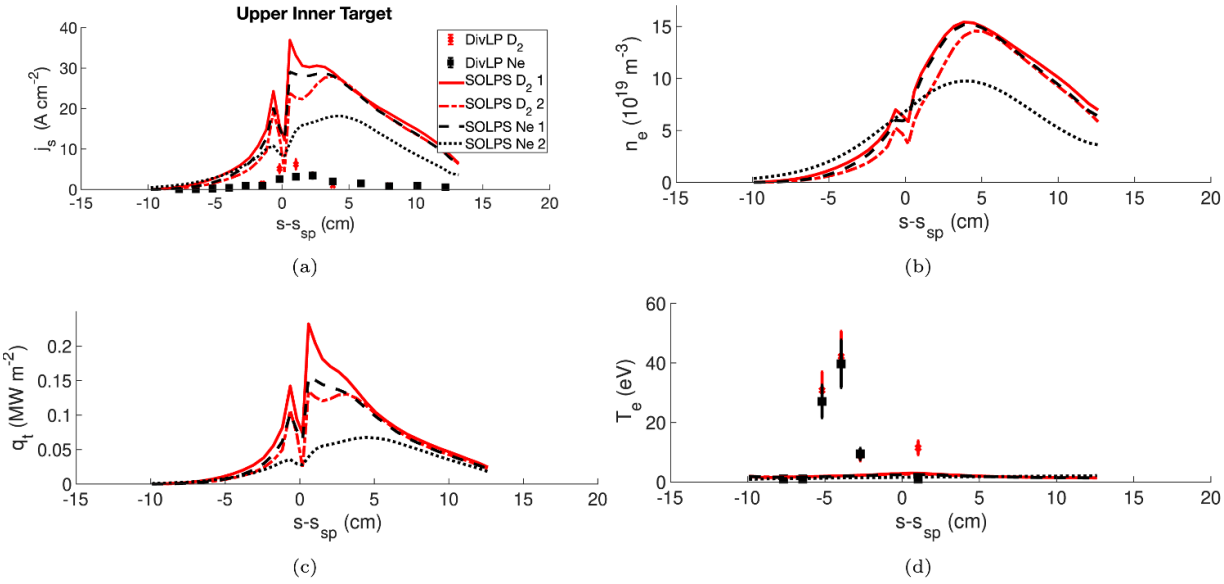

Figure 9. The profiles of the ion saturation current (*a*), density (*b*), heat flux (*c*) and temperature (*d*) at the UIT during the purely deuterium and the neon seeded discharge.

For this disagreement between simulations and experiments at the UIT a couple of remarks should be taken into account. First, the quality of the DivLP data at the UIT was not as good as the quality at the UOT making a general overview more challenging. Secondly, it is known that the anomalous transport at the inboard side can differ from the one at the outboard side [24] which is not taken into account in the performed analysis. Simulations were performed in which the anomalous diffusion in the entire divertor region was raised. This increased indeed the maximum temperature at the UIT, but decreased it at the UOT. However, a large increase in anomalous transport is needed to cover the temperature difference. A more in-depth study of the difference in anomalous transport between UIT and UOT is left for future work.

In the following sections first the effect of drifts on the observed profiles is examined with the SOLPS-ITER simulations and later the effects of the neon on the radiation and the plasma–neutral interactions are discussed. Where the upstream and downstream analysis is a combination of experimental data and simulations, the following sections are mainly based on the performed SOLPS-ITER simulations. The presented up- and downstream agreement can be seen as the way to reflect the reality in the simulations as good as possible due to the lack of further experimental data for these particular experiments.

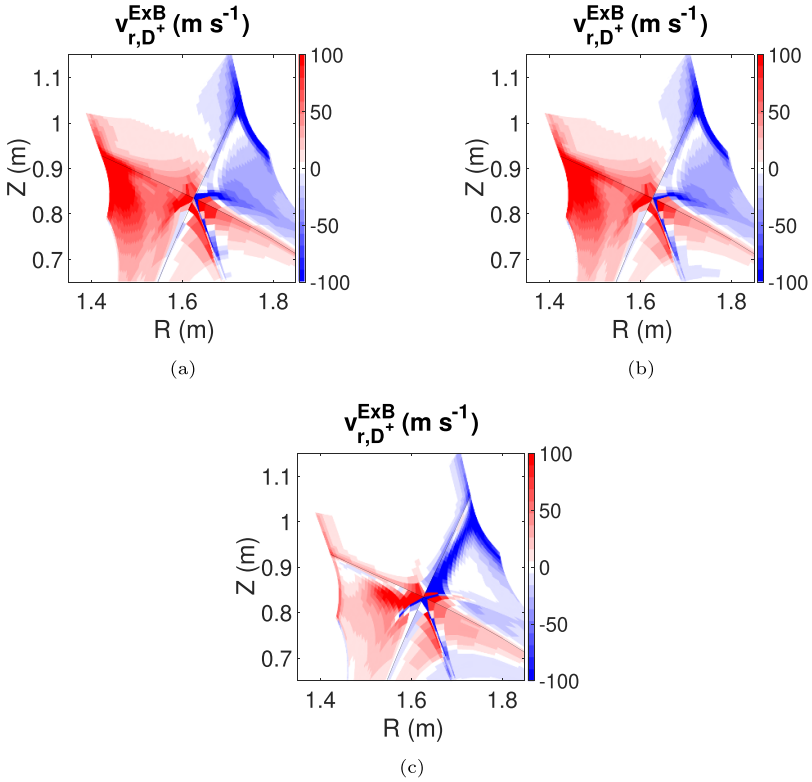

Figure 10. The $E \times B$ drift velocity of D^+ in the radial direction shown for the 'SOLPS D_2 1' (*a*), 'SOLPS Ne 1' (*b*) and 'SOLPS Ne 2' (*c*) simulations in the vicinity of the divertor. The separatrix in all plots is indicated in black.

4. Effects of drift on deuterium and neon transport

The analysis of the drifts effects is performed for the 'SOLPS D_2 1', 'SOLPS Ne 1', and 'SOLPS Ne 2' simulations. The 'SOLPS Ne 1' simulation makes it possible to study the effect of neon itself, where the 'SOLPS Ne 2' simulation helps to understand what we observed during the experiments.

This study includes the combined effect of $E \times B$ drifts and diamagnetic drifts. Drifts in SOLPS-ITER have been studied widely in literature. Nevertheless, it is the first time that their effect on neon seeded simulations for EAST are studied. Therefore, appendix gives an overview of how the effect of the high field side high density, double-peaked plasma profiles at the targets, and in–out divertor asymmetry is present in the studied simulations. In this section the focus is rather on the effect of drifts on the ionization location and stagnation point, both on the one of deuterium as the one of neon.

Figure 10 shows for all the simulated cases that the radial $E \times B$ drift velocity changes sign between UIT and UOT. In this figure, positive means towards the SOL, where negative means towards the private flux region (PFR). At the UIT this causes that the ionization location shifts further into the SOL, where at the UOT this shifts towards the separatrix with its peak value just into the SOL as can be seen in figure 11. As an additional D_2 puff is added in the 'SOLPS Ne 1' simulation (as part of the D_2–Ne injection), this effect is more pronounced over there in comparison with the 'SOLPS D_2 1' simulation. At the inner divertor, due to the low T_e at the UIT itself, the ionization profiles mainly change further away from the target towards the divertor entrance. Over there, a clear shift of the ionization into the SOL region in comparison with a simulation without drifts is observed which explains the large j_s UIT values in the SOL region in the simulations.

The redistribution of the particle due to the $E \times B$ drifts, causes in ASDEX Upgrade and JET, a high density region in the inner divertor [25]. The relative importance of drifts can be quantified by the ratio of the parallel particle flux to the outer divertor and the $E \times B$ flux towards the PFR part of the inner divertor [26]. Table 3 gives this ratio for the performed simulations. This indicates that for the 'SOLPS D_2 1' simulation around 16% of the flux arriving at the UOT is redistributed to the UIT due to the $E \times B$ drifts. The inclusion of neon in the simulation reduces the effect of drifts. This can also be seen in figure 28 where the differences between non-drift and drift simulations are reduced for the 'SOLPS Ne 1' simulation. The importance of drifts is nearly vanishing in simulation 'SOLPS Ne 2' due to the increased anomalous transport profiles in the PFR and divertor region for that simulation.

The density scan in figure 12 shows that the 'SOLPS D_2 1' and 'SOLPS Ne 1' simulations are still attached and have not yet reached the rollover despite the low temperatures at the UIT. The 'SOLPS Ne 2' simulation, on the other hand, has a decreasing particle flux when the density is further increased, so is detached at the UIT. A similar analysis shows that also the UOT in this last simulation is detached. The other simulations are attached at the UOT. As detachment is going together with a larger density, it is not surprising that the later simulation has the highest density profiles at the UIT (see figure 8(*b*)). Drifts

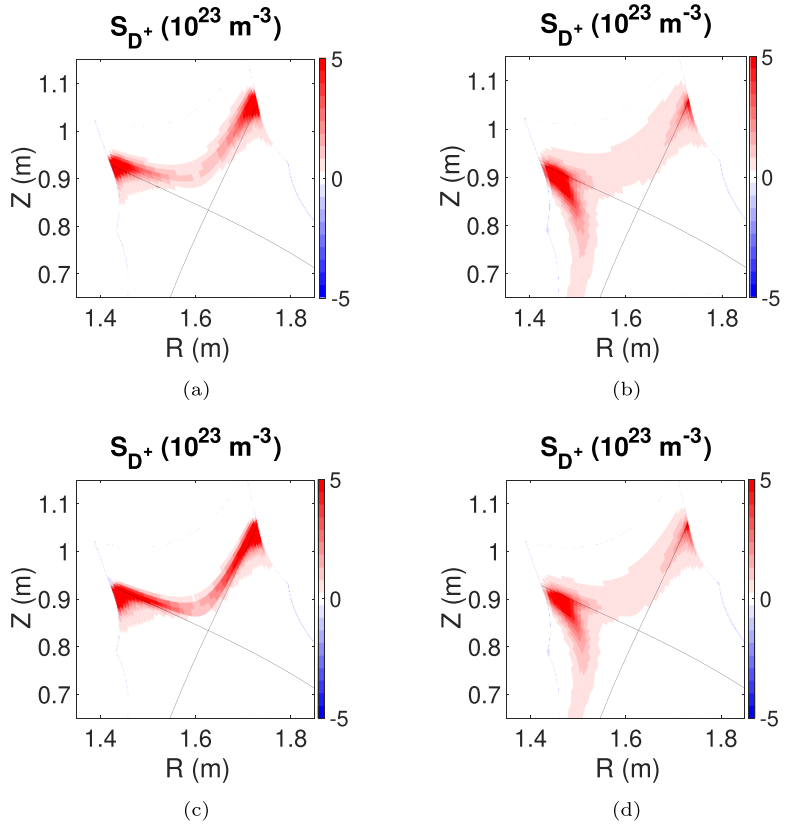

Figure 11. The ionization source for D^+ in the vicinity of the divertor region in the 'SOLPS D_2 1' and 'SOLPS Ne 1' simulations without (*a*), (*c*) and with (*b*), (*d*) drifts.

Table 3. The relative importance of the $E \times B$ flows.

	$\frac{\Gamma^{\mathrm{UIT,PFR}}_{E\times B}}{\Gamma^{\mathrm{UOT}}_{\parallel}}$
SOLPS D_2 1	0.1627
SOLPS Ne 1	0.1175
SOLPS Ne 2	∼0

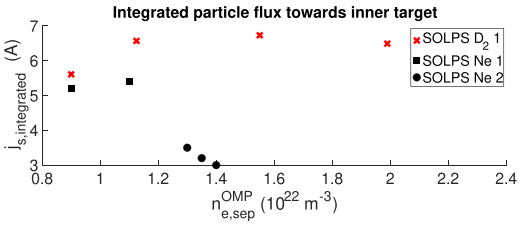

Figure 12. A density scan to study the degree of detachment for the different simulation setups. The original simulation is the most left point on the plot for all setups.

in fact increase the ionization sources at the inboard side as can be seen in figure 11.

Another way to study the redistribution from particles between the inner and outer target due to drift effects, is the analysis of the flow direction and flow reversal. In figures 13 the evolution of the parallel velocity for D^+ is studied for the 'SOLPS D_2 1' and 'SOLPS Ne 2' simulations. The velocity profile for the 'SOLPS Ne 1' simulation is very similar to the one of 'SOLPS D_2 1'. Similar plots for Ne^+ and Ne^{8+} in the presence of drifts are shown in figures 14 and 15. When the velocity is zero, the studied ion is not moving in the parallel direction and a stagnation point appears. A positive velocity implies that the plasma particles are moving towards the UIT, while a negative one indicates they are moving towards the UOT.

Figure 13 shows that in the absence of drifts, the parallel velocity pattern is nearly symmetric and particles move towards the closest target. Drift effects change this picture completely. $B\nabla B$ flows influence the velocity pattern mainly in the main SOL where $E \times B$ flows influence the parallel velocity pattern mainly in the PFR and divertor region. Figure 13 shows that in the detached simulation 'SOLPS Ne 2', there is the largest shift in movement towards the inner target. Due to the magnetic curvature, most particles will escape from the core towards the SOL around the position of the OMP. Figure 13(*d*) indicates that most of these particles flow towards the inner target in the 'SOLPS Ne 2' simulation, where this influence is smaller in the absence of drifts.

In cases with impurities, the stagnation point of the impurity ions, in combination with the ionization location will also indicate if there is retention of the impurity in the divertor region, or if there is more leakage towards the SOL and to the core [27]. The mechanism behind this, is a balance of drifts and friction with the main ions. The OMP-to-target impurity flux ratio is determined by the fraction of impurity neutrals ionized beyond the stagnation point, with these impurities being

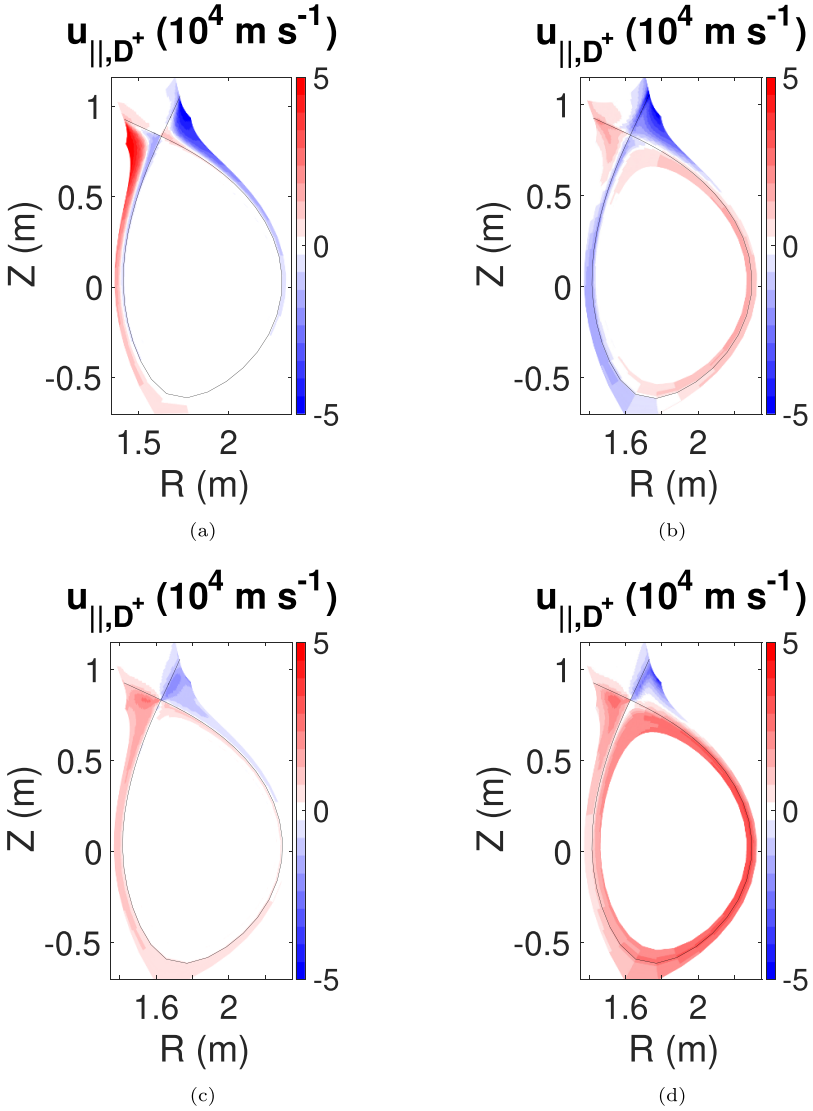

Figure 13. The parallel velocity of D^+ for the different simulations: 'SOLPS D_2 1' without (*a*) and with (*b*) drifts, and 'SOLPS Ne 2' without (*c*) and with (*d*) drifts. The separatrix in all figures is indicated in black.

carried upstream by friction with the main ions as described in [27]. As drifts strongly influence the poloidal velocity profile of the main ions (see figure 13), they also influence the one of the impurities. Figures 14 and 15 indicate that the asymmetry of the impurity velocities increases when the charge state is higher.

The densities for Ne^+ and Ne^{8+} are shown in figure 16. The density profiles (not exact values) are similar at most locations between the 'SOLPS Ne 1' and 'SOLPS Ne 2' simulations, apart from the Ne^{8+} density in the vicinity of the target, where there is a peak in density at the UOT for 'SOLPS Ne 1', there is rather a peak at the UIT in the 'SOLPS Ne 2' simulation. The significant larger parallel velocity of Ne^{8+} shown in figure 15 indicates that in the later simulation more of the Ne^{8+} is transported to the inner target. This causes also a different location for the ionization of Ne^{8+}. These ionization sources, as well as the ones for Ne^+ are given in figure 17. For the low charge states of neon, the ionization is located in the entire edge, where the higher charge states ionize more towards the core. Figure 14 makes clear that there is a large region where the parallel velocity of Ne^+ is close to zero. Figure 17 shows that ionization of Ne^+ is taking place within this region. In that way, the transport mechanism described above will make that Ne^+ leaks towards the core. As there the temperature increases, the higher charge states of neon ionizes inside the separatrix as is the case for Ne^{8+}.

The location of the ionization sources for Ne^+ agrees with observations in other devices of similar size. Also in [19, 26, 28] for ASDEX Upgrade modeling the ionization location at the inner target extends further than at the outer target. For larger devices, like ITER, on the other hand, this extension is not present [28]. A difference with ASDEX Upgrade, on the other hand, is the proximity of the ionization front of Ne^+ to the inner target in figure 17(*a*). For ASDEX Upgrade modeling, this is located closer towards the X-point and only for larger devices like JET the ionization fronts moves towards the target. In the detached simulation 'SOLPS Ne 2', however,

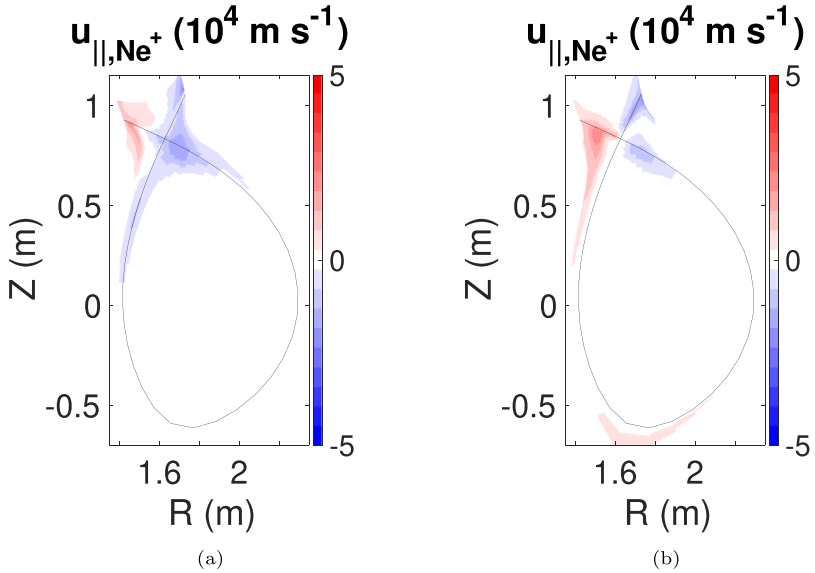

Figure 14. The parallel velocity of Ne^{+} for the different simulations: 'SOLPS Ne 1' (*a*), and 'SOLPS Ne 2' (*b*). The separatrix in all figures is indicated in black.

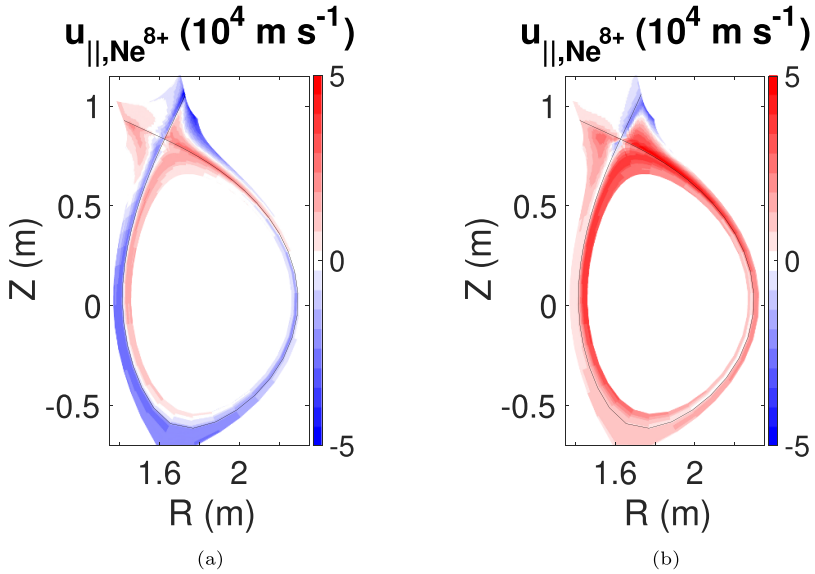

Figure 15. The parallel velocity of Ne^{8+} for the different simulations: 'SOLPS Ne 1' (*a*), and 'SOLPS Ne 2' (*b*). The separatrix in all figures is indicated in black.

figure 17(*b*) shows that the peak in Ne^{+} ionization is more inwards. Reference [26] shows for ASDEX Upgrade the presence of Ne ions mainly at the inner target, but also in the core. By combining the profiles of figures 16(*a*) and (*c*), it is clear that this also holds for the presented EAST simulations.

However, the small influence of neon on the experimental T_e profiles of figure 9(*d*) indicates that the transport of neon towards the inner target is overestimated in the simulations. The leakage of higher order charge states of Ne is nevertheless confirmed by the EUV spectrometer data from figure 2(*d*). The chords of the EUV spectrometer are going through the core in order to view the divertor region so they include the core content as well.

5. Effect of neon on radiated power fraction

The main goal of the injected neon is to radiate a significant power fraction and in that way detach the plasma.

The total radiated power for the different simulations is displayed in figure 18. This radiated power exists of line radiation which is only a major contributor to the total radiation if neon is added to the simulation (figure 19), Bremsstrahlung (negligible for all performed simulations), radiation due to atoms, molecules and molecular ions which are referred to as neutral radiation (figure 20), and in the case of simulations 'SOLPS D_2 2' and 'SOLPS Ne 2' also artificial radiation (figure 21). Where simulation 'SOLPS D_2 1' and 'SOLPS Ne 1' have only

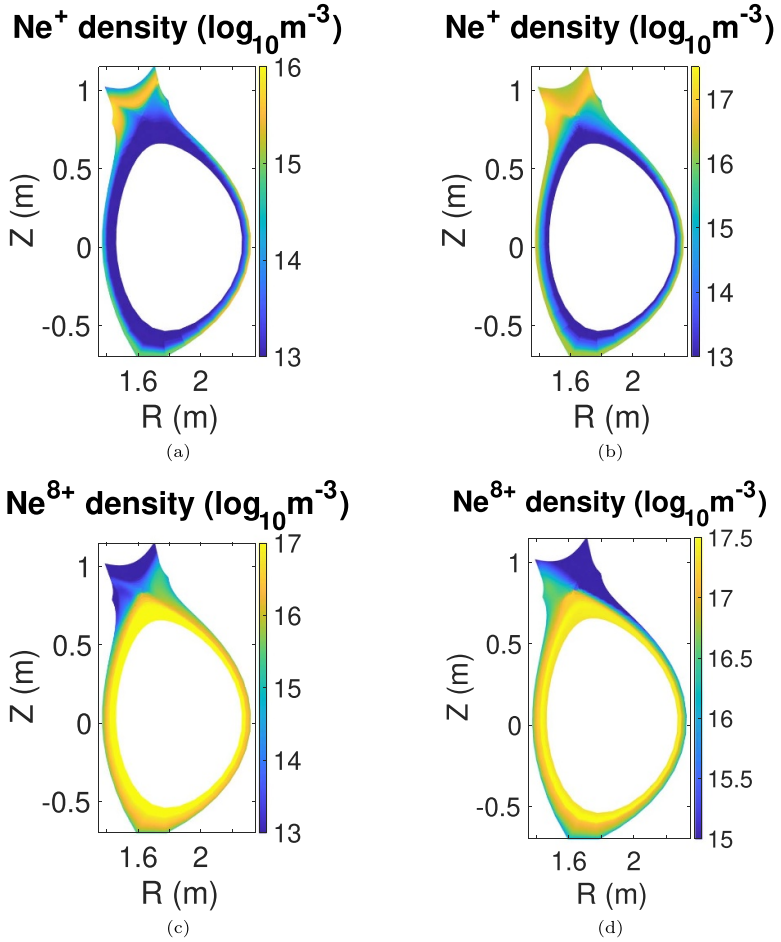

Figure 16. The densities for Ne^{+} and Ne^{8+} simulated with SOLPS-ITER for 'SOLPS Ne 1' (*a*), (*c*) and 'SOLPS Ne 2' (*b*), (*d*).

a radiation peak in the vicinity of the inner target, simulations 'SOLPS D_2 2' and 'SOLPS Ne 2' show a larger radiation region including the region around the X-point. Figure 21 shows that a large contribution is caused by this artificial radiation. Table 4 indicates that artificial radiation contributes 32% of the radiated power in the 'SOLPS Ne 2' simulation. As described in section 3 artificial radiation is a simplified model to describe radiation from impurities which are not included as separate impurity species in the SOLPS-ITER simulation. The experimental divertor profiles at the UOT from figure 8 could only be obtained by introducing this artificial radiation in the simulation. The used 1% of artificial radiation gave the best agreement with the experimental data in the 'SOLPS Ne 2' simulation. This suggest that the presence of other radiators besides neon is important to drive the plasma into detachment for an EAST-size device with tungsten wall. This is in agreement with the observation at ASDEX Upgrade that pure neon seeding experiments over there are unstable [8] and can only be stabilized when neon injection is combined with another impurity like nitrogen [29].

Apart from the other impurities, figure 19 shows the effect of neon. Especially in the 'SOLPS Ne 2' simulation, neon is causing radiation around the X-point and along the outer divertor leg. For the neon itself, line radiation is the main radiation mechanism. This line radiation is the one which is aimed for by impurity cooling. The location of the line radiation for simulation 'SOLPS Ne 2' is similar to earlier experimental findings at JET [8, 10] and SOLPS-ITER modeling for ASDEX Upgrade and JET [26, 28]. As shown in [30] the exact location of the maximum radiation (inside or outside the separatrix) can be influenced by the amount of added neon, but the overall behavior is similar to the one observed in simulations 'SOLPS Ne 1' and 'SOLPS Ne 2'. Both at ASDEX Upgrade and at JET, the puff location is located in the PFR where at EAST two puff locations are present: one at the OMP for D_2 and one at the upper outer strikeline for the D_2/Ne mixture. As shown in [31] the location of the main ion injection can influence the radiation location.

Bremsstrahlung is in all simulations very small and is never a major contributor to the total radiated power fraction.

The neutral radiation shown in figure 20 is the main contributor to the 'SOLPS D_2 1' and 'SOLPS Ne 1' simulations. This neutral radiation is originating from neutral friction between the deuterium ions and neutral particles (see figure 1) and will happen at temperatures of $T_e \sim 2-5$ eV in the divertor region as neutrals are present over there (in contrast to the

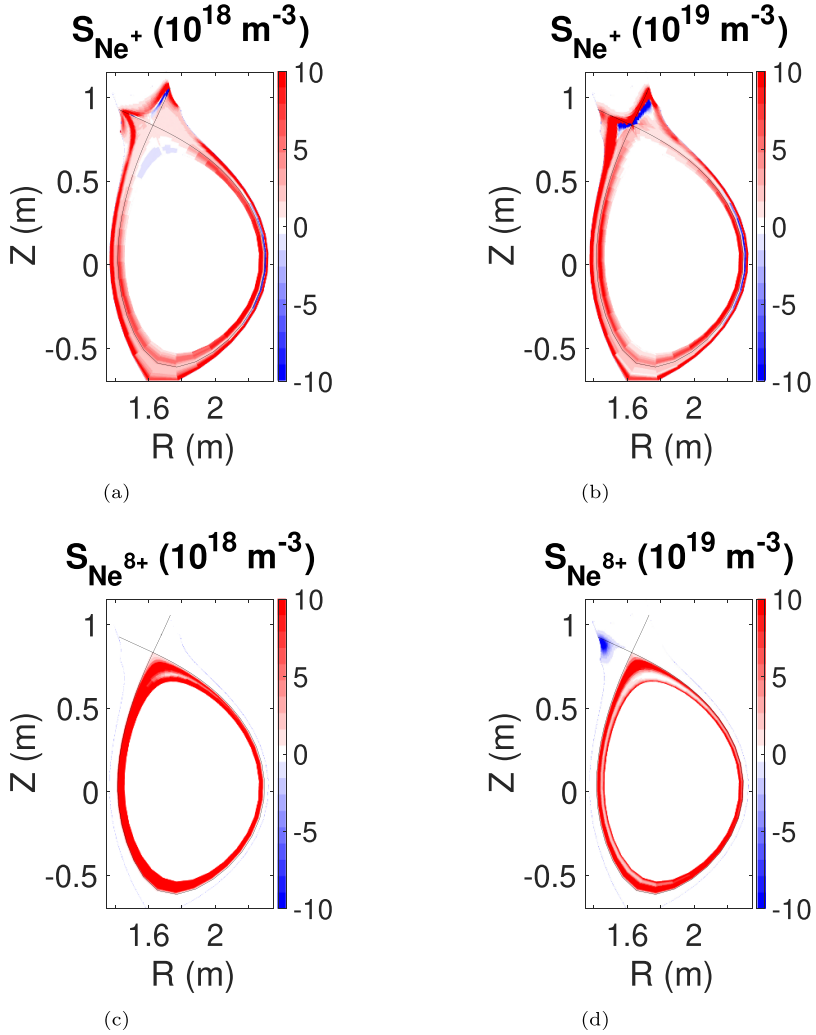

Figure 17. The ionization sources from neutral to Ne^{+} and from Ne^{7+} to Ne^{8+} simulated with SOLPS-ITER for 'SOLPS Ne 1' (*a*), (*c*) and 'SOLPS Ne 2' (*b*), (*d*).

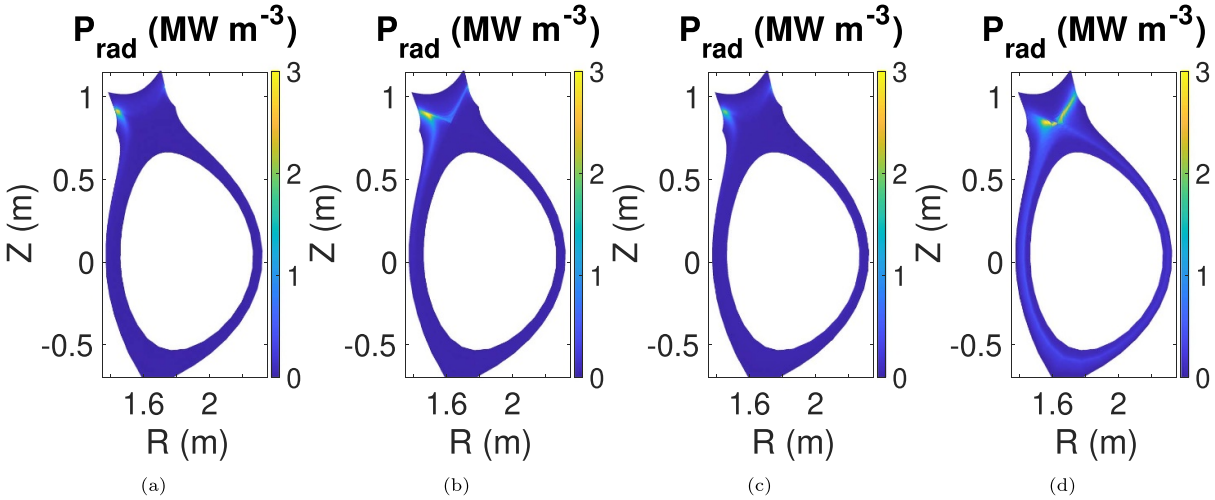

Figure 18. The simulated radiated power profiles for the SOLPS D_2 1 (*a*), SOLPS D_2 2 (*b*), SOLPS Ne 1 (*c*) and SOLPS Ne 2 (*d*) simulations.

Table 4. The radiated power fractions for the performed SOLPS-ITER simulations.

	SOLPS D_2 1	SOLPS D_2 2	SOLPS Ne 1	SOLPS Ne 2
P_{in}	2.05 MW	2.05 MW	1.8 MW	1.77 MW
P_{rad}	0.174 MW	0.375 MW	0.232 MW	0.986 MW
$P_{art\,rad}$	0 MW	0.228 MW	0 MW	0.317 MW
$P_{line\,rad}$	∼0 MW	∼0 MW	0.0699 MW	0.504 MW
P_{Brem}	∼0 MW	∼0 MW	∼0 MW	0.001 89 MW
$P_{neut\,rad}$	0.174 MW	0.146 MW	0.161 MW	0.163 MW
f_{rad}	8.5%	18%	13%	55.7%

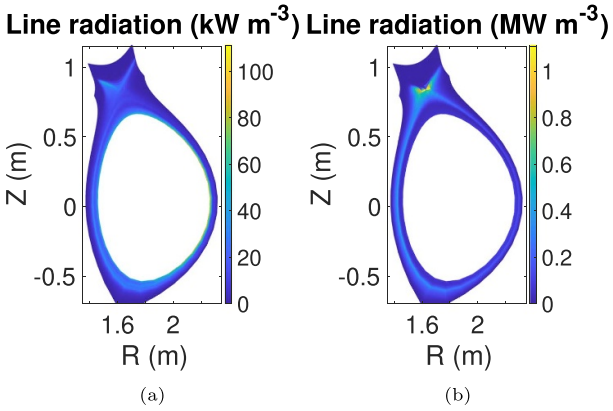

Figure 19. The simulated line radiation profiles for the SOLPS Ne 1 (*a*) and SOLPS Ne 2 (*b*) simulations. For the purely deuterium simulations the contribution of line radiation is negligible. Notice that the color scales are different.

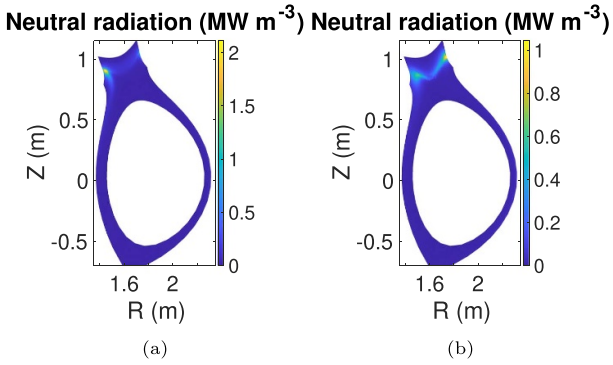

Figure 20. The simulated neutral radiation profiles for the SOLPS Ne 1 (*a*) and SOLPS Ne 2 (*b*) simulations. The neutral radiation pattern for SOLPS D_2 1 (∼25% higher) and SOLPS D_2 2 (∼25% lower) are similar to the one of SOLPS Ne 1. Notice that the color scales are different.

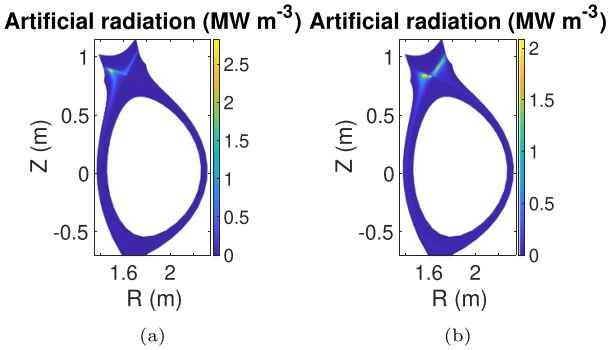

Figure 21. The simulated artificial radiation profiles for the SOLPS D_2 2 (*a*) and SOLPS Ne 2 (*b*) simulations. Notice that the color scales are different.

rest of the SOL). This plasma–neutral friction is important to obtain the necessary conditions for volumetric recombination, but does not contribute to the reduction of the flux to the targets [32]. Another way to see where this peak in neutral radiation is to be expected is from the location of deuterium ionization of figure 11 which shows a peak at the same location. For 'SOLPS D_2 1', 'SOLPS D_2 2' and 'SOLPS Ne 1' this is the case in the vicinity of the inner target, where for 'SOLPS Ne 2' figure 8(*d*) shows that the plasma temperatures are also decently low around the UOT separatrix. This, in combination with the additional gas puff over there, makes that there is not only a peak in neutral radiation around the UIT but also at the UOT.

Figure 18 has shown the differences in radiation pattern between the different performed simulations. However, in order to avoid overheating of the divertor targets, the remaining question is which percentage of the power entering the SOL is radiated in the edge. This is shown in table 4. This demonstrates the large influence of the 1% 'artificial' impurity content on the overall radiation: in the deuterium simulation, this more than doubles the radiated power. As shown in figure 12, only the 'SOLPS Ne 2' simulation is detached. This also becomes clear from the radiative power fraction. The SOLPS-ITER simulations for ASDEX Upgrade and ITER of [26] required similar percentages of radiated power fraction to bring the discharge in detachment.

As the AXUV measurement of figure 2(*c*) is mainly looking to core radiation and as all filterscope chords of figure 2(*d*) pass through the core, it is difficult to make a dedicated radiation analysis based on the available experimental data. Nevertheless, the DivLP profiles at the UOT (figure 8) and the D_α signal over there from the filterscope show that there was an influence of neon during the experiment.

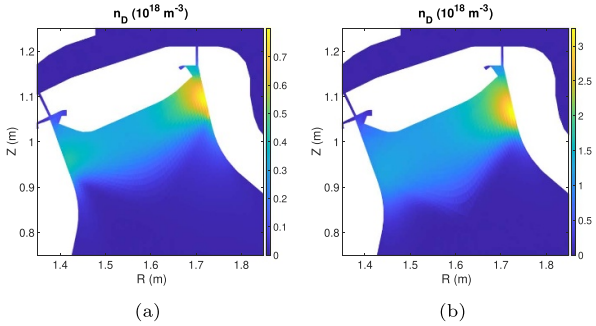

Figure 22. The neutral deuterium atom density in the 'SOLPS D_2 1' (*a*) and 'SOLPS Ne 2' (*b*) simulations in the divertor region. Remark the difference in the colorbar between the two density profiles.

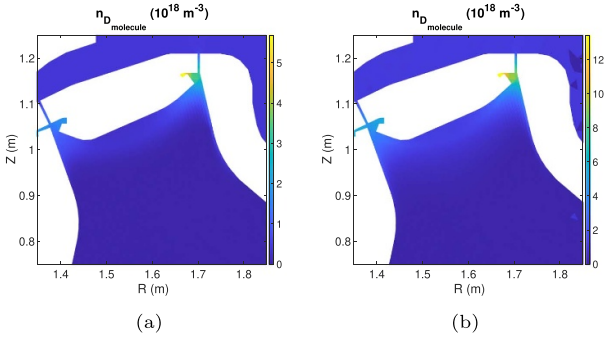

Figure 23. The neutral deuterium molecule density in the 'SOLPS D_2 1' (*a*), and 'SOLPS Ne 2' (*b*) simulations in the divertor region. The profiles of the neutral deuterium molecule density for the 'SOLPS D_2 2' (slightly lower) and 'SOLPS Ne 1' (similar) simulations are similar to the one for the 'SOLPS D_2 1' simulation. Remark the difference in colorbar between the two density profiles.

6. Influence of neutral transport

Neutral processes play an important role in the divertor region where the plasma temperatures are low, plasma densities are high, and where there is an influx of neutrals from recycling and gas injection [5, 33]. Table 1 shows the neutral reactions which are included in the performed SOLPS-ITER modeling. The molecular hydrogen originates from the gas puff at the OMP and at the UOT strikepoint for the neon-seeded simulations, and from recycling at the walls. Apart from such surface recombination, the atomic hydrogen results from elastic collisions, ionizing dissociation or charge exchange. In EIRENE, the recycling of deuterium (and neon) at the tungsten divertor target, or the carbon first wall, is calculated using the TRIM database [34]. Apart from this PWI, table 1 lists the resulting products of a particular reaction. In the neon seeded simulations, an additional neon ionization reaction from the AMJUEL database [35] and neon recombination from the ADAS database [36] are included. The neutral neon originates from the neon injection at the UOT strikeline, and due to recombination of Ne ions.

In section 4 it was already shown that ionization plays an important role in explaining the plasma behavior. The ionization location of deuterium is mainly driven by a combination of PWI and the plasma quantities in the divertor region. In figure 22 the neutral deuterium atom density is shown for the 'SOLPS D_2 1' and 'SOLPS Ne 2' simulations. The atom densities from the other simulations are similar to the ones of the 'SOLPS D_2 1' simulation. Where the atom density is largely increasing due to the added injection of a deuterium/neon mixture in the vicinity of the UOT, the main change in ionization takes place at the UIT (see figure 11). In the absence of the D_2–Ne injection, the main driver of deuterium atom generation is PWI.

Where the atom density is similar for all simulations apart from 'SOLPS Ne 2', the location of largest molecular density stays similar, but the maximum one increases with a factor ∼4 between the 'SOLPS D_2 1' and 'SOLPS Ne 2' simulations (see figure 23). Also remark that the maximum molecular density is always higher than the maximum atom one but is located further away from the strike line towards the subdivertor region where it cannot react with plasma anymore. Looking to the table of included neutral reactions (table 1) it is concluded that the PWI is the driver for the deuterium molecule density.

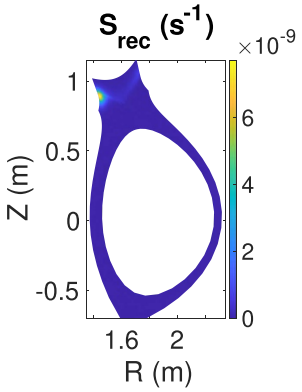

Figure 24. The neutral source rate of deuterium atoms in the 'SOLPS Ne 2' simulation due to recombination.

The elastic collision reactions have a small impact due to the size of EAST. As the mean free path of neutral-neutral reactions is long in comparison to the tokamak size, they do not contribute much to the plasma physics [15]. Also the atomic and plasma particle and energy source terms originating from charge exchange reactions appeared to be very small in the studied simulations.

The recombination of deuterium has a negligible impact, both in the purely deuterium and in the neon seeded simulation. This is shown for the particle sources for atomic deuterium due to recombination in the 'SOLPS Ne 2' simulation in figure 24. Here it can be seen that recombination only plays a small role at the UIT. Comparison of the target profiles of a 'SOLPS Ne 2' simulation with and without recombination switched on confirms the small effect of recombination as indicated in figure 25 for the j_s and n_e profiles at the UIT. This is in agreement with what can be expected from the target profiles of figures 8 and 9: the lowest electron temperature is obtained at the UIT, and even this one is ∼1.8 eV. In figure 1 it was indicated that temperatures below ∼1 eV are required to allow recombination to play an effective role.

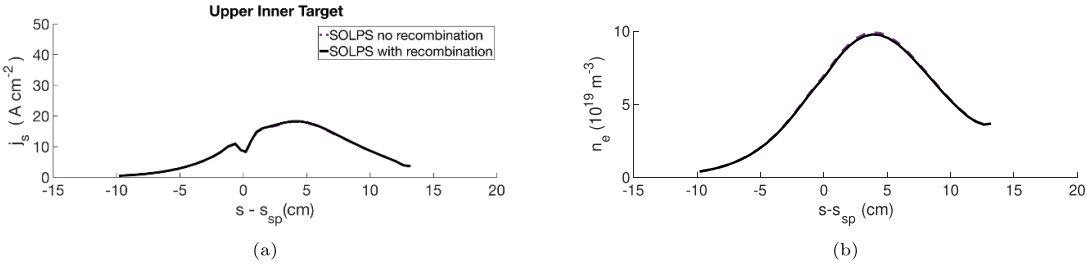

Figure 25. The limited impact of the inclusion of recombination reactions on the j_s (a) and n_e profiles at the UIT.

The atomic data of [35, 37] show that the cross-section for the density levels obtained in the 'SOLPS Ne 2' simulation result in $\sim 5\,10^{-13}$cm^3 s^{-1} where for an electron temperature of 0.1 eV, this would result in $\sim 10^{-9}$cm^3 s^{-1}.

The small effect of deuterium recombination is also confirmed by the low line radiation of deuterium. The recombination of neon in the 'SOLPS Ne 1' and especially in the 'SOLPS Ne 2' simulations, on the other hand, has a larger effect resulting in larger levels of line radiation in the vicinity of the targets where the temperature is low as shown in figures 19(a) and (b). Due to the low density of neon in comparison with deuterium, their impact on the plasma profiles is, however, limited.

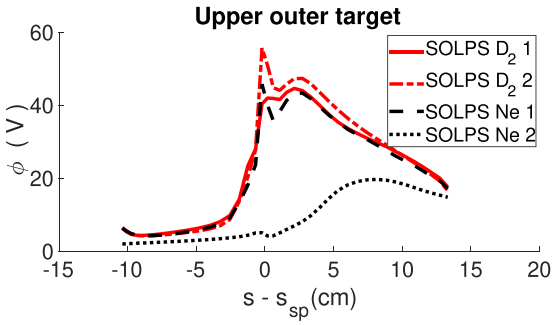

Figure 26. The potential at the UOT for all the performed SOLPS-ITER simulations.

7. Discussion

The main question to be answered in this work is the influence of neon on the plasma edge transport. Edge transport in SOLPS-ITER is dominated by four mechanisms: anomalous transport which is originating from turbulence, drifts, radiation, and neutral interactions [38]. These mechanisms are the drivers for the physics that particles can undergo and which was shown in figure 1. We now want to know the influence of neon on these mechanisms and on the physical processes.

Figure 8 shows that only with modified anomalous transport in comparison with purely deuterium simulations it is possible to match the UOT profiles of the neon seeded experiment. For the performed neon simulation which matched best the experimental conditions at the UOT (SOLPS Ne 2), the transport was reduced in the SOL, but increased in the divertor and PFR regions. This increased transport in the divertor and PFR region causes a decrease in potential in the vicinity of the targets and especially around the separatrix as shown for the UOT in figure 26. This makes that in the detached neon seeded simulation (SOLPS Ne 2) the double peaking for the target profiles vanished as can be seen in figures 9 and 8.

Apart from the divertor target profiles, the clearest influence of neon is observed in the radiation data. Due to a large increase in line radiation, the total radiation and in that way the energy losses the ions experience on their way towards the divertor target increases in comparison with the purely deuterium case. Comparing simulations 'SOLPS D_2 2' and 'SOLPS Ne 2' on the other hand shows that the neutral radiation around the UIT is decreasing. This is caused by the reduced deuterium ionization which is clear from comparing figure 27 with figure 11(b).

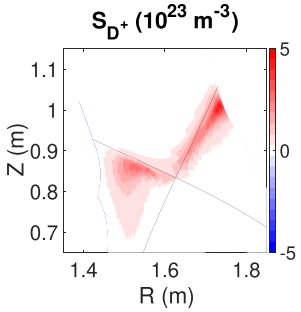

Figure 27. The ionization source for D^+ in the vicinity of the divertor region in the 'SOLPS Ne 2' simulation.

The leakage from Ne towards the core in combination with the cooling down of the core due to the ionization of higher charge states of neon explains why it was not possible to perform H-mode experiments with a higher neon injection. Core radiation is mainly coming from Bremsstrahlung and line radiation. Figure 19 shows that, especially for simulation 'SOLPS Ne 2', the peak in line radiation in the edge where figure 17 shows that ionization of larger charge states of Ne is happening at the core boundary of the SOLPS-ITER grid. As a result this leakage causes the ionization to be the main energy sink in the core.

To come back to figure 1, the neon ions radiate around the X-point and cause in that way additional loss terms to the energy equation. When looking to the outer target, for which the simulations are matched better with experimental data in comparison with the inner target, there will be a larger influence of the neutral friction as the deuterium ionization sources increase. Right in front of the target, the recombination of neon

causes further radiation losses which are visible in the line radiation in figure 19(*b*). The influence of deuterium recombination, on the other hand, is very small because of the larger temperatures.

To summarize, analysis of neon in the vicinity of the UOT shows that neon influences the radiated power fraction, decreases the deuterium ionization, increases the neutral friction, but does not manage to cause deuterium recombination.

8. Summary and conclusion

In the presented paper neon seeding experiments, performed at EAST in the campaign of 2019 in USN configuration, are taken as a starting point for SOLPS-ITER modeling to evaluate the effect of neon seeding on plasma edge transport in EAST.

Several SOLPS-ITER simulations are analyzed to study the effect of neon in EAST. First, a reference, purely deuterium simulation is considered. In a next step, neon is added to this simulation for which the amount of neon is matched with the experimental input from 2019. This, however, did not match the experimental profiles. Therefore, a second neon seeded simulation is analyzed in which the transport, neon injection, and radiation behavior of other species is changed as such to have better agreement with the experimental observations. These simulations have similar profiles as the experiments at the UOT and at the OMP. At the upper inner target, on the other hand, the simulated temperatures are an order of magnitude smaller than in the experiments as no varying anomalous transport between inner and outer divertor is used. Therefore, the focus of the performed analysis is on the neon effects at the midplane and outer divertor region.

Where the purely deuterium and initial neon-seeded simulations are attached, the final neon-seeded simulation shows a rollover in particle flux, so can be used to study detachment in EAST. In the analysis it is shown that the drift flows are essential to determine the location where the ionization will take place and in that way determine the particle sources. Drifts increase the ionization sources on the inboard side due to an increased particle flow towards the inner target.

By analyzing the behavior of the Ne ions, it is shown that Ne^{+} leaks towards the core. This makes Ne-seeding experiments with sufficient Ne to bring the discharge into full detachment challenging and causes that higher order states of neon ionize and in that way radiate in the core.

Due to neon, a shift in radiated power from neutral radiation to line radiation is observed. On top, the radiated power fraction more than triples for the simulation which fits best to the experimental data. The analysis suggests that the presence of other radiative species besides Ne is needed to explain the detachment behavior of EAST-size devices.

At the UOT, there is a decrease in temperature and an increase in density, but the cross-section of the deuterium recombination reaction stays very low. At the inner target, the simulations experience a very small influence of recombination in the target profiles.

This analysis shows that neon has a strong impact on the plasma edge transport, but that it remains difficult to confirm the simulated advantages with experiments.

Acknowledgments

The authors would like to thank Niels Horsten and Petra Börner for their help with all EIRENE-related questions.

The authors would like to thank Xavier Bonnin for his help with SOLPS-ITER-related questions.

This work has been carried out within the framework of the EUROfusion Consortium, funded by the European Union via the Euratom Research and Training Programme (Grant Agreement No. 101052200 - EUROfusion). Views and opinions expressed are however those of the author(s) only and do not necessarily reflect those of the European Union or the European Commission. Neither the European Union nor the European Commission can be held responsible for them.

This work was funded in parts by the College of Engineering at UW Madison, WI, USA

This work is supported by the National Key R&D Program of China under Contract No. 2024YFE03270700, and program of National Natural Science Foundation of China under Contract No. 12305250.

The SOLPS-ITER simulations were performed at the Marconi supercomputer from the National Supercomputing Consortium CINECA.

Appendix. Effect of drifts in comparison with observed effect in other devices

This appendix shows the influence of drifts on the simulated plasma profiles compared to earlier observations on other devices. Figure 28 shows the influence of activating the $E \times B$ and diamagnetic drifts in SOLPS-ITER at the targets.

As studied in [25] for ASDEX Upgrade, the shift in peak of the target profiles is caused by the $E \times B$ drift flows. These flows cause additional particle sources in the far SOL. Figure 29 shows the $E \times B$ drift velocities for the different simulations. Due to the definition of the computational grid, a positive velocity implies that the plasma particles are moving towards the UIT, while a negative one indicates they are moving towards the UOT. Where the $E \times B$ drift velocities in the PFR stay limited (especially further away from the separatrix), they indeed have a larger impact in the SOL.

For simulations 'SOLPS D_2 1' and 'SOLPS Ne 1', there appears a double peak in the j_s profile due to drifts. Part of these oscillations in plasma profiles around the separatrix can be explained by numerical effects (see [16]). However, a double peaking is also observed in other experimental and computational EAST studies [39] as well as in DIII-D, TCV, ASDEX Upgrade... [40]. For the performed simulations, the profile of the $E \times B$ drift velocities in the vicinity of the divertor targets explain this double peaking. Figure 29 indicates small regions around the UIT and UOT separatrix where the direction of

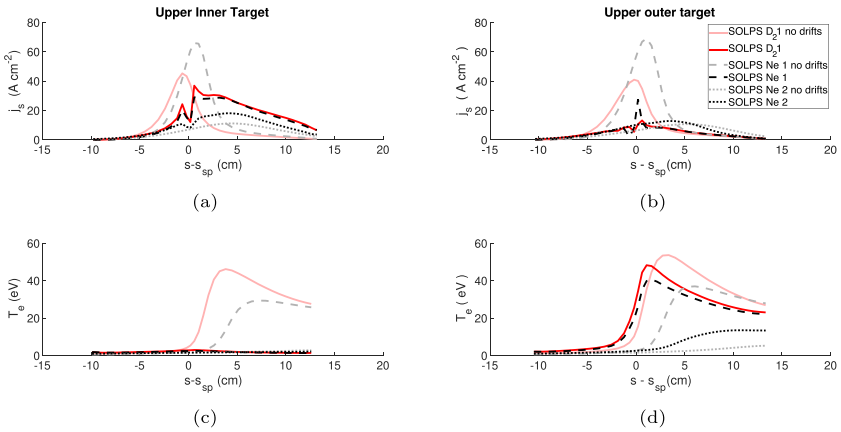

Figure 28. The influence of drift flows on the electron temperature and ion saturation current profiles at the divertor targets.

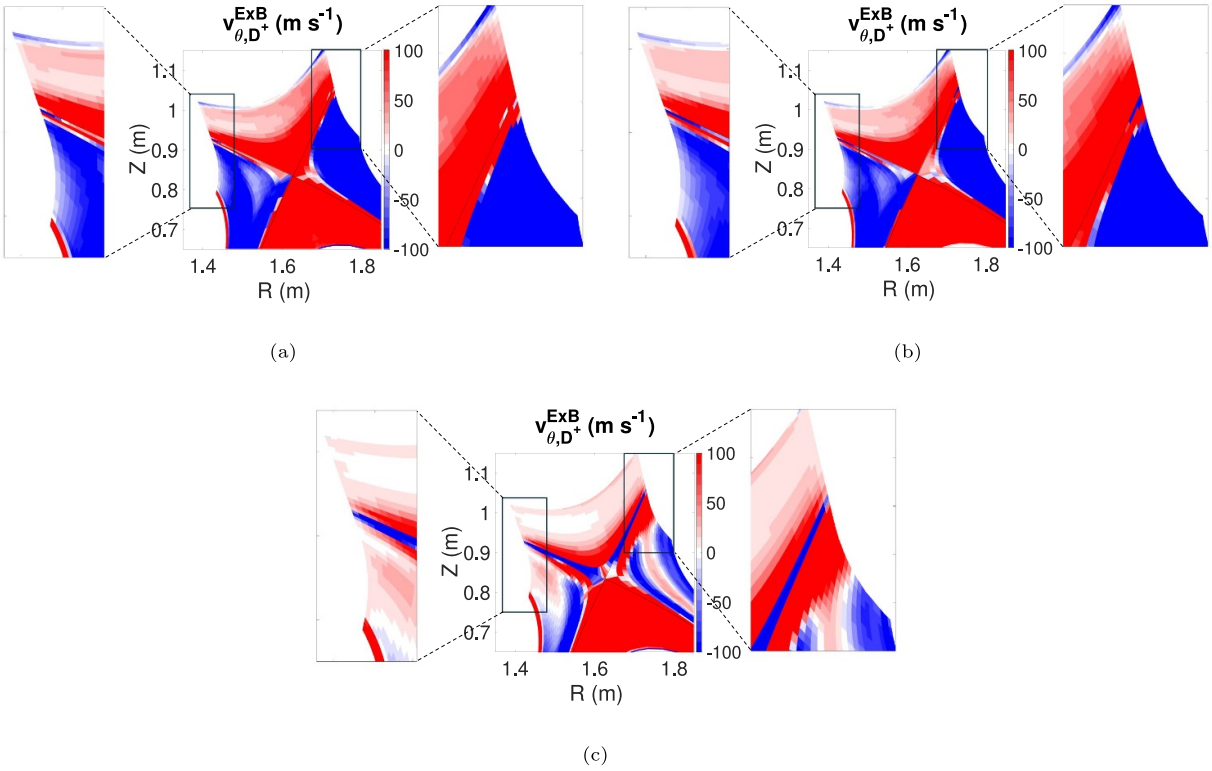

Figure 29. The $E \times B$ drift velocity of D^+ in the poloidal direction shown for the 'SOLPS D_2 1' (*a*), 'SOLPS Ne 1' (*b*) and 'SOLPS Ne 2' (*c*) simulations in the vicinity of the divertor. The separatrix in all plots is indicated in black.

the $E \times B$ drift velocity is changed. These regions agree with the location of a peak (UOT) or the location of a valley in between the two peaks (UIT). The different behavior between UOT and UIT corresponds with the additional drift flow in the SOL which transports particles from the inboard to the outboard side as also observed in [39]. It explains why the double peak is observed at the inner target and two valleys are present at the outer target. Figure 29(*b*) shows that the effect is larger at the UOT in the 'SOLPS Ne 1' simulation in comparison with the 'SOLPS D_2 1' one. In the vicinity of the inner target, figure 29(*b*) indicates that the region of reversed $E \times B$ velocity penetrates deeper into the plasma when neon is added to the simulation. The effect on the particle flux (figure 28(*a*)) stays however limited.

Reference [30] points out that this double peaking vanishes when the transport in the PFR and divertor region is increased. In simulations 'SOLPS Ne 2', the anomalous diffusion in the divertor region, is three times larger than in the other simulations, and as can be seen on figure 28, this simulation does not show a double peaking. Figure 29(*c*) confirms that here the influence of the $E \times B$ ion velocity is smaller than in the other simulations.

The radial drift velocities of figure 10 explain the shift in maximum plasma quantities at the UOT from further into the

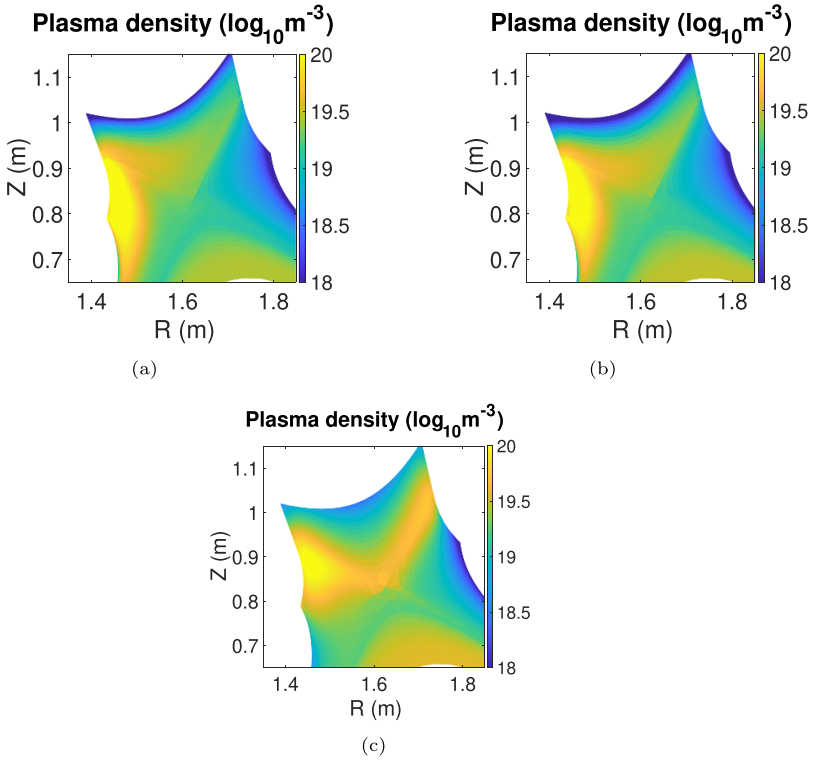

Figure 30. The simulated 2D density profiles in the vicinity of the divertor region for the SOLPS D_2 1 (*a*), SOLPS Ne 1 (*b*) and SOLPS Ne 2 (*c*) simulations.

SOL towards the separatrix. As drifts do not only transport particles, but also momentum and energy, their influence is not only limited to the n_e profiles, but also the T_e profiles are influenced. Due to the double peaking/the valley the observed shift is less pronounced for the j_s profiles than for the T_e ones. The shift in peaked T_e shifts the location where more energy is present as well as the ionization location of D^+. This change in ionization location explains the shift in peak value of j_s at the targets. At the UOT the peak shifts closer towards the separatrix for the Ne-seeded simulations where no clear shift is observed for the purely deuterium simulation. At the UIT, the shift in peak for j_s is less pronounced, but if it is observed, it moves away from the separatrix into the SOL.

These redistributions cause that the inner divertor becomes detached where the outer one stays attached, and is called the high field side high density. From figure 30 it is clear that a higher density is present at the inboard side for all the performed EAST simulations.

ORCID iDs

Dieter Boeyaert 0000-0003-0920-8660
Stefano Carli 0000-0001-6581-2745
Wouter Dekeyser 0000-0003-1954-3729
Sven Wiesen 0000-0002-3696-5475
Liang Wang 0000-0002-8373-117X
Fang Ding 0000-0001-5886-8847
Kedong Li 0000-0003-0486-7368
Yunfeng Liang 0000-0002-9483-6911
Martine Baelmans 0000-0001-9905-4583

References

[1] Pacher G., Pacher H., Janeschitz G., Kukushkin A., Kotov V. and Reiter D. 2007 Modelling of DEMO core plasma consistent with SOL/divertor simulations for long-pulse scenarios with impurity seeding *Nucl. Fusion* **47** 469
[2] Wiesen S. *et al* 2017 Plasma edge and plasma-wall interaction modelling: lessons learned from metallic devices *Nucl. Mater. Energy* **12** 3–17
[3] Fenstermacher M. *et al* 1999 Physics of the detached radiative divertor regime in DIII-D *Plasma Phys. Control. Fusion* **41** A345
[4] Leonard A. 2018 Plasma detachment in divertor tokamaks *Plasma Phys. Control. Fusion* **60** 044001
[5] Krasheninnikov S. and Kukushkin A. 2017 Physics of ultimate detachment of a tokamak divertor plasma *J. Plasma Phys.* **83** 155830501
[6] Pitcher C.S. and Stangeby P. 1997 Experimental divertor physics *Plasma Phys. Control. Fusion* **39** 779
[7] Stangeby P.C. *et al* 2000 *The Plasma Boundary of Magnetic Fusion Devices* vol 224 (Institute of Physics Publishing)
[8] Bernert M. *et al* 2017 Power exhaust by SOL and pedestal radiation at ASDEX Upgrade and JET *Nucl. Mater. Energy* **12** 111–8
[9] Kallenbach A. *et al* 2013 Impurity seeding for tokamak power exhaust: from present devices via ITER to DEMO *Plasma Phys. Control. Fusion* **55** 124041
[10] Glöggler S. *et al* 2019 Characterisation of highly radiating neon seeded plasmas in JET-ILW *Nucl. Fusion* **59** 126031
[11] Wu S. (EAST Team) 2007 An overview of the EAST project *Fusion Eng. Des.* **82** 463–71
[12] Wiesen S. *et al* 2015 The new SOLPS-ITER code package *J. Nucl. Mater.* **463** 480–4
[13] Bonnin X., Dekeyser W., Pitts R., Coster D., Voskoboynikov S. and Wiesen S. 2016 Presentation of the

new SOLPS-ITER code package for tokamak plasma edge modelling *Plasma Fusion Res.* **11** 1403102
[14] Boeyaert D., Wiesen S., Wischmeier M., Dekeyser W., Carli S., Wang L., Ding F., Li K., Liang Y. and Baelmans M. (EAST Team) 2021 Towards assessment of plasma edge transport in neon seeded plasmas in disconnected double null configuration in EAST with SOLPS-ITER *Nucl. Mater. Energy* **26** 100926
[15] Boeyaert D., Carli S., Ghoos K., Dekeyser W., Wiesen S. and Baelmans M. 2022 Numerical error analysis of SOLPS-ITER simulations of EAST *Nucl. Fusion* **63** 016005
[16] Boeyaert D., Carli S., Dekeyser W., Wiesen S. and Baelmans M. 2024 Numerical implications of including drifts in SOLPS-ITER simulations of EAST *Phys. Plasmas* **31** 023905
[17] Zang Q., Zhao J., Yang L., Hu Q., Xi X., Dai X., Yang J., Han X., Li M. and Hsieh C. 2011 Upgraded multipulse laser and multipoint Thomson scattering diagnostics on EAST *Rev. Sci. Instrum.* **82** 063502
[18] Reiter D., Baelmans M. and Boerner P. 2005 The EIRENE and B2-EIRENE codes *Fusion Sci. Technol.* **47** 172–86
[19] Senichenkov I.Y., Poletaeva A., Kaveeva E., Veselova I.Y., Nichik A. and Rozhansky V. 2025 Comparison of divertor seed impurity gases retention efficiency by SOLPS-ITER modeling *Nucl. Fusion* **65** 056042
[20] Xu J. *et al* 2016 Upgrade of Langmuir probe diagnostic in ITER-like tungsten mono-block divertor on experimental advanced superconducting tokamak *Rev. Sci. Instrum.* **87** 083504
[21] Mao H. *et al* 2017 The impacts of lithium and silicon coating on the W source in EAST *Nucl. Mater. Energy* **12** 447–52
[22] Pan O. *et al* 2022 SOLPS-ITER simulations of an X-point radiator in the ASDEX Upgrade tokamak *Nucl. Fusion* **63** 016001
[23] Sun G. *et al* 2025 Investigating the influence of divertor baffles on nitrogen-seeded detachment in TCV with SOLPS-ITER simulations and TCV experiments *Nucl. Fusion* **65** 026061
[24] Reimold F. 2014 Experimental studies and modeling of divertor plasma detachment in H-mode discharges in the ASDEX Upgrade tokamak *PhD Thesis* Technische Universität München - Faculty of physics
[25] Reimold F. *et al* 2017 The high field side high density region in SOLPS-modeling of nitrogen-seeded H-modes in ASDEX Upgrade *Nucl. Mater. Energy* **12** 193–9
[26] Sytova E., Pitts R.A., Kaveeva E., Bonnin X., Coster D., Rozhansky V., Senichenkov I., Veselova I., Voskoboynikov S. and Reimold F. 2019 Comparing N versus Ne as divertor radiators in ASDEX-Upgrade and ITER *Nucl. Mater. Energy* **19** 72–78
[27] Senichenkov I.Y. *et al* 2019 On mechanisms of impurity leakage and retention in the tokamak divertor *Plasma Phys. Control. Fusion* **61** 045013
[28] Rozhansky V., Kaveeva E., Senichenkov I., Veselova I., Voskoboynikov S., Pitts R., Coster D., Giroud C. and Wiesen S. 2021 Multi-machine SOLPS-ITER comparison of impurity seeded H-mode radiative divertor regimes with metal walls *Nucl. Fusion* **61** 126073
[29] Henderson S. *et al* 2023 Divertor detachment and reattachment with mixed impurity seeding on ASDEX Upgrade *Nucl. Fusion* **63** 086024
[30] Kaveeva E., Rozhansky V., Veselova I., Senichenkov I., Giroud C., Pitts R.A., Wiesen S. and Voskoboynikov S. 2021 SOLPS-ITER drift modelling of JET Ne and N-seeded H-modes *Nucl. Mater. Energy* **28** 101030
[31] Park J.-S., Bonnin X., Pitts R. and Lore J. 2024 Impact of gas injection location and divertor surface material on ITER fusion power operation phase divertor performance assessed with SOLPS-ITER *Nucl. Fusion* **64** 036002
[32] Krasheninnikov S., Kukushkin A. and Pshenov A. 2016 Divertor plasma detachment *Phys. Plasmas* **23** 055602
[33] Janev R., Post D., Langer W., Evans K., Heifetz D. and Weisheit J. 1984 Survey of atomic processes in edge plasmas *J. Nucl. Mater.* **121** 10–16
[34] Eckstein W. and Heifetz D. 1987 Data sets for hydrogen reflection and their use in neutral transport calculations *J. Nucl. Mater.* **145** 332–8
[35] Reiter D. *et al* 2000 The data file AMJUEL: additional atomic and molecular data for EIRENE Forschungszentrum Juelich GmbH 52425
[36] Summers H. and O'Mullane M. 2011 Atomic data and modelling for fusion: the ADAS project *AIP Conf. Proc.* **1344** 179–87
[37] Sawada K. and Fujimoto T. 1995 Effective ionization and dissociation rate coefficients of molecular hydrogen in plasma *J. Appl. Phys.* **78** 2913–24
[38] Schneider R., Bonnin X., Borrass K., Coster D., Kastelewicz H., Reiter D., Rozhansky V. and Braams B. 2006 Plasma edge physics with B2-Eirene *Contrib. Plasma Phys.* **46** 3–191
[39] Jia G. *et al* 2022 Role of $E\times B$ drift in double-peak density distribution for the new lower tungsten divertor with unfavorable B_t on EAST *Nucl. Fusion* **62** 056005
[40] Colandrea C. 2024 Investigation of scrape-off layer and divertor transportusing infrared thermography and SOLPS-ITER simulations *PhD Thesis* École Polytechnique de Lausane